UNIVERSITY OF BATH

Citation for published version:
Benton, C & Mitchell, CN 2011, 'Isolating the multipath component in GNSS signal-to-noise data and locating reflecting objects', Radio Science, vol. 46, RS6002. https://doi.org/10.1029/2011RS004767

DOI:
10.1029/2011RS004767

Publication date:
2011

Link to publication

An edited version of this paper was published by AGU. Copyright 2011 American Geophysical Union.
Benton, C. J., and C. N. Mitchell (2011), Isolating the multipath component in GNSS signal-to-noise data and locating reflecting objects, Radio Sci., 46, RS6002, doi:10.1029/2011RS004767

University of Bath

Isolating the multipath component in GNSS signal-to-noise data and locating reflecting objects

C. J. Benton[1] and C. N. Mitchell[1]

[1] A filter to separate the effect of multipath in Global Navigation Satellite System (GNSS) signal-to-noise ratio (SNR) data is presented. The filter removes multipath cleanly, and affects neither slowly varying trends (such as tropospheric absorption or variation in satellite range) nor high frequency components (such as ionospheric scintillation), and so is potentially useful in space-weather research. Similarly, the multipath data removed from the input data is minimally distorted, and contains useful information as to the multipath geometry. A method to locate reflecting objects using a form of spectral analysis is described.

1. Introduction

[2] Multiple-path (multipath) effects are a source of both problems and opportunities for Global Navigation Satellite System (GNSS) applications. (The term "multipath" is used here to describe any form of not-line-of-sight reception; it does not imply that multiple reflections are occurring.) Whilst the most severe problem is that of a receiver locking onto a reflected or diffracted signal, causing a spurious increase in measured satellite range [*Kaplan and Hegarty*, 2006], a variety of more subtle effects will occur even when the receiver is correctly locked onto the direct signal.

[3] One such effect (and the focus of this paper) is the influence on the signal-to-noise ratio (SNR) recorded by the receiver, in which alternating intervals of constructive and destructive interference between the direct and reflected signals cause quasi-periodic oscillations. The SNR oscillation effect can be disruptive or beneficial, depending on application. For example, in ionospheric research, amplitude scintillation (i.e. rapid variation in observed amplitude) is a routinely measured quantity. Multipath distorts these measurements by adding another source of amplitude variations [*Van Dierendonck et al.*, 1993]. Conversely, in the case of ground-reflected multipath, SNR oscillations have been used to determine soil moisture content [*Larson et al.*, 2008a, 2008b, 2010]. A SNR derived assessment of multipath may also be used to compensate for its effect on other quantities, such as the observed phase of the carrier wave [*Axelrad et al.*, 1994, 1996; *Bilich et al.*, 2007].

[4] In both cases, it is desirable to isolate the SNR variation due to multipath, so that it may either be discarded or analyzed in further detail. In section 2, such a filter scheme is presented. Similarly, regardless of whether multipath is disruptive or beneficial, it is useful to determine (or verify) the location of the reflecting object. In section 3, a technique to constrain the reflector location is presented.

[5] Finally, in section 4, results for three different multipath scenarios, all using Global Position System (GPS) data, are presented. These consisted of an antenna in a relatively simple multipath environment, an antenna in a very complex multipath environment, and an antenna on coastal cliffs, where the sea acted as the reflector.

2. Multipath Isolation Filter

[6] A range of schemes have been used for removing or extracting multipath effects from SNR data. When multipath is to be analyzed, wavelet filters have been used [*Bilich and Larson*, 2007; *Bilich et al.*, 2008], as have schemes which combine the SNR data from multiple antennas [*Comp and Axelrad*, 1998]. When amplitude scintillation is to be measured, multipath effects (amongst other things) are commonly removed by dividing the signal by the output of a low-pass filter [*Van Dierendonck et al.*, 1993]. Kalman filters (and various derivatives thereof) based on multipath models have also been used [*Dai et al.*, 1997].

[7] Such techniques exploit the fact that the physical effects combining to give the measured SNR have different characteristic frequencies. The movement of the satellite causes a slow variation in SNR, due to the changing satellite distance, and the antennas (of both satellite and receiver) having direction-dependent gain. Signal absorption in the troposphere (which is particularly high at low satellite elevations) will cause a similar slow variation. These effects will occur at periods of many hours.

[8] Power fluctuations due to ionospheric scintillation are conventionally held to start at frequencies above 0.1 Hz, which is a standard cutoff-frequency for the "detrending" filters used in ionospheric research [*Van Dierendonck et al.*, 1993; *Beach and Kintner*, 1999; *Forte*, 2005]. In practice, this can often be

[1]Department of Electronic and Electrical Engineering, University of Bath, Bath, UK.

increased to 0.3 Hz, especially at higher latitudes, where the Fresnel frequencies are generally higher [*Forte*, 2005].

[9] The multipath oscillation (for a single locally-planar reflector) occurs at a frequency ν given (as derived in section 3.1) by

$$\nu = \frac{2\xi}{\lambda} |\vec{v} \cdot \hat{w}| \qquad (1)$$

where λ is the wavelength, $\vec{v}$ is a vector pointing to (and perpendicular to) the plane of the reflector, ξ is the apparent angular velocity of the satellite across the sky, and $\hat{w}$ is a unit vector (perpendicular to the vector pointing towards the satellite) giving its apparent direction of motion.

[10] The highest multipath frequencies occur for distant reflectors. This is increased for grazing-incidence reflection, which corresponds to $\vec{v}$ and $\hat{w}$ being roughly parallel. Assuming that $\vec{v}$ and $\hat{w}$ are exactly parallel, that $|\vec{v}| = 250$ m (which encompasses the most distant reflector used in the examples below, specifically the sea beneath a coastal cliff), that $\xi = 1.45 \times 10^{-4}$ rad s^{-1} (corresponding to the approximately 12 hour orbital period), and that $\lambda = 19.05$ cm (the L1 wavelength), gives an upper frequency of 0.4 Hz. This can potentially overlap with ionospheric scintillation, but in practice such large values are extreme cases, which are only relevant to antennas placed in the shadow of large hills [*Bilich and Larson*, 2007] or above unusually high coastal cliffs. These extremes require the distant reflector to be very large, in order to overcome the weakening in signal due to the inverse square law. Reducing $|\vec{v}|$ to a more likely maximum of 50 m keeps the multipath frequency below 0.1 Hz.

[11] Low multipath frequencies occur for nearby reflectors. The lowest possible frequency of multipath is formally zero, which occurs when the vector $\vec{v}$ is precisely aligned with the direction of the satellite, giving $\vec{v} \cdot \hat{w} = 0$. This, however, will only last for a short period of time, and for most geometries will not happen at all. Assuming that the satellite never comes within 5° of perfect alignment, then an extremely close reflector at $|\vec{v}| = 1$ m will have a minimum frequency of 0.5 cycles per hour, which is higher than that of the above slowly varying trends.

[12] Therefore, in most cases, the multipath will be within a range of fading frequencies that is higher than the slowly varying trend, but lower than ionospheric scintillation, and so can be isolated.

2.1. Derivation of Filter

[13] A new multipath filter scheme was derived by modeling the phenomenon, and then constructing a network of digital filters to systematically deconstruct the resulting equation and extract the relevant terms.

[14] It was assumed that power measurements were mean values taken over time intervals equal to the 20 ms C/A (coarse acquisition) data-bit length (or multiples thereof), causing the contribution from frequency components other than the carrier to effectively sum to zero. The power itself was assumed to be a constant multiple of the recorded SNR (at least for a given receiver over a single satellite pass). The ideal interference pattern between a sine-wave of wavelength λ and its reflections will be of the form

$$P_0 \left[1 + \sum_n \rho_n \cos\left(\frac{2\pi}{\lambda} d_n\right) \right]^2 \qquad (2)$$

where (for the nth reflection) d_n is the difference in path length and ρ_n is a slowly varying parameter depending on the reflectance. The reflection of electromagnetic waves is normally accompanied by a half-cycle phase shift, and so ρ_n will usually be negative.

[15] The radiation pattern of the antenna will also influence ρ_n, as the direct and reflected signals will often arrive in directions with different gain. Furthermore, if the antenna is circularly polarized, the reversal of handedness that the signal undergoes on reflection will also cause a gain difference. This is unproblematic if multipath is simply to be removed, as the only constraint on ρ_n is that it is slowly varying, and so the fact that it conflates two physical effects is irrelevant. It is also (as explained in section 3.2), unimportant when determining reflector location. It only becomes necessary to know the antenna gain pattern if the reflectance itself is to be measured.

[16] This form was generalized to give a model for power P as

$$P = P_0 Q \left[1 + \sum_n \rho_n \cos\left(2\pi \frac{d_n}{\lambda}\right) \right]^2 (1 + s) \qquad (3)$$

The slowly varying trends in SNR are represented by Q. This is roughly proportional to $G_r G_s T / r^2$, where r is the distance to the satellite, T is the fraction of transmitted power reaching the receiver, G_r is the antenna gain the receiver (in the direction of the satellite), and G_s is the antenna gain of the satellite (in the direction of the receiver). These factors do not have to be considered separately, as the only requirement made of Q is that it be slowly varying. For convenience, Q is defined to have a mean value of 1, which is achieved by appropriate choice of the power unit P_0.

[17] The $(1 + s)$ factor accounts for rapid variation in power (due to effects such as ionospheric scintillation). This is the sum of the mean power (scaled to 1 by choice of P_0), and a high-frequency term s, which represents the variation about this mean.

[18] Equation (3) therefore consists of a low frequency factor Q, an intermediate frequency factor $[1 + \sum_n \rho_n \cos(2\pi d_n/\lambda)]^2$ and a high frequency factor $(1 + s)$. Each of these factors tends towards a value of one if the physical effects being represented are removed. This suggests that they can be separated using a homomorphic (or cepstrum) filter $\mathcal{H}$, which is a filter applied to logarithmic data. (Homomorphic analysis has been used in the analysis of GPS multipath before [*Ying et al.*, 2003; *Wang et al.*, 2008], but not as part of the filter scheme described here.) A homomorphic filter splits the signal up as

$$P = P_0 P_{\mathcal{H}(\omega < \omega_1)} P_{\mathcal{H}(\omega_1 < \omega < \omega_2)} P_{\mathcal{H}(\omega_2 < \omega)} \qquad (4)$$

where $P_{\mathcal{H}(\omega_2 < \omega)}$, $P_{\mathcal{H}(\omega_1 < \omega < \omega_2)}$ and $P_{\mathcal{H}(\omega < \omega_1)}$ are dimensionless variables giving the high, middle and low frequency components. The corner frequencies ω_1 (low) and ω_2 (high) are chosen to encompass the frequency range of the multipath oscillation. Making the change of variables $W \equiv \ln (P/P_0)$, $W_{\mathcal{H}(\omega < \omega_1)} \equiv \ln (P_{\mathcal{H}(\omega < \omega_1)})$, $W_{\mathcal{H}(\omega_1 < \omega < \omega_2)} \equiv \ln (P_{\mathcal{H}(\omega_1 < \omega < \omega_2)})$ and $W_{\mathcal{H}(\omega_2 < \omega)} \equiv \ln (P_{\mathcal{H}(\omega_2 < \omega)})$ transforms equation (4) to

$$W = W_{\mathcal{H}(\omega < \omega_1)} + W_{\mathcal{H}(\omega_1 < \omega < \omega_2)} + W_{\mathcal{H}(\omega_2 < \omega)} \qquad (5)$$

and equation (3) to

$$W = \ln(Q) + 2\ln\left[1 + \sum_n \rho_n \cos\left(2\pi\frac{d_n}{\lambda}\right)\right] + \ln(1+s) \quad (6)$$

In this logarithmic form, the homomorphic filters become linear filters $\mathcal{L}$.

[19] Terms of the form $f = \ln(1 + \alpha \cos\theta)$ will include frequency components besides that of the multipath oscillation. These can be analyzed by noting that f is approximately periodic, and so can be represented as a Fourier series, with the fundamental frequency being equal to that of the power oscillation. The periodicity is only approximate, as both the multipath frequency and ρ_n vary with time. However, the time scales of these variations are much longer than the time period of individual oscillations, and so periodicity can be assumed over short time intervals. In practical terms, it is required that periodicity is a good approximation over durations up to the digital filter correlation length.

[20] The ω_1 corner frequency is (by definition) lower than the multipath frequency, and so the effect of the ω_1 low pass filter will be to isolate the zeroth order (constant) term f_0 from the series. For a single reflector, this can be evaluated (for constant α) as

$$f_0(\alpha) \equiv \frac{1}{2\pi}\int_{-\pi}^{\pi}\ln(1+\alpha\cos\theta)\,d\theta = \ln\left(\frac{1+\sqrt{1-\alpha^2}}{2}\right) \quad (7)$$

In the case of multiple reflectors this term generalizes (see Appendix A) to

$$f_0(\alpha_1, \alpha_2, \cdots, \alpha_n) = \sum_n \ln\left(\frac{1+\sqrt{1-\alpha_n^2}}{2}\right) \quad (8)$$

The Fourier series of $\ln(1 + \alpha\cos\theta)$ will also contain higher order terms, with frequencies equal to integer multiples of the multipath frequency. These can usually be removed by giving ω_2 a value substantially larger than the multipath frequency, thus filtering out the strongest harmonics.

[21] Similarly, the fact that s contains only high frequency components, does not imply that the same is true for $\ln(1+s)$. However, assuming the spectral width of s is relatively narrow, the spectrum of $\ln(1+s)$ will consist of a comb of frequency peaks, spaced at integer multiples of the central frequencies of s. The peaks of this comb will pass on either side of the $\omega_1 < \omega < \omega_2$ frequency band, and so $\ln(1+s)_{\mathcal{L}(\omega_1<\omega<\omega_2)}$ will be small.

[22] Applying the filters (and making the above assumptions) gives

$$W_{\mathcal{H}(\omega<\omega_1)} = \ln(Q) + 2\sum_n f_0(\rho_n) + \ln(1+s)_{\mathcal{L}(\omega<\omega_1)} \quad (9)$$

$$W_{\mathcal{H}(\omega_1<\omega<\omega_2)} = 2\ln\left[1 + \sum_n \rho_n \cos\left(2\pi\frac{d_n}{\lambda}\right)\right] - 2\sum_n f_0(\rho_n) \quad (10)$$

$$W_{\mathcal{H}(\omega_2<\omega)} = \ln(1+s)_{\mathcal{L}(\omega_2<\omega)} \quad (11)$$

Transforming out of the logarithmic basis gives

$$P_{\mathcal{H}(\omega_1<\omega<\omega_2)} = \left(\prod_n \frac{2}{1+\sqrt{1-\rho_n^2}}\right)^2 \left[1 + \sum_n \rho_n \cos\left(2\pi\frac{d_n}{\lambda}\right)\right]^2 \quad (12)$$

Taking the square root of the central component (and expanding) gives

$$\sqrt{P_{\mathcal{H}(\omega_1<\omega<\omega_2)}} = \left(\prod_n \frac{2}{1+\sqrt{1-\rho_n^2}}\right) + \quad (13)$$

$$\left(\prod_n \frac{2}{1+\sqrt{1-\rho_n^2}}\right)\sum_n \rho_n \cos\left(2\pi\frac{d_n}{\lambda}\right) \quad (14)$$

where the first term is slowing varying, whilst the second term is rapidly varying. Therefore, using high and low pass linear filters $\mathcal{L}$ about the ω_1 frequency, and dividing defines a quantity

$$\Theta \equiv \frac{\left[\sqrt{P_{\mathcal{H}(\omega_1<\omega<\omega_2)}}\right]_{\mathcal{L}(\omega_1<\omega)}}{\left[\sqrt{P_{\mathcal{H}(\omega_1<\omega<\omega_2)}}\right]_{\mathcal{L}(\omega<\omega_1)}} = \sum_n \rho_n \cos\left(2\pi\frac{d_n}{\lambda}\right) \quad (15)$$

which is the sum of multipath oscillations, modulated by their reflection coefficients. Therefore a quantity $\widetilde{P}$ can be defined

$$\widetilde{P} \equiv \frac{P}{(1+\Theta)^2} = P_0 Q(1+s) \quad (16)$$

which is equivalent to equation (3) with all the multipath reflection terms ρ_n set to zero.

[23] In summary, the filter scheme acts (assuming the above assumptions hold) to split the input data into two quantities. The first quantity Θ describes the multipath (and nothing but the multipath), whilst the second quantity $\widetilde{P}$ is the multipath-free data. The input data can be trivially reconstructed as $P = \widetilde{P}(1+\Theta)^2$, and so the filter is reversible.

2.2. Numerical Implementation of the Filter

[24] The system was implemented using the algorithm outlined in Figure 1. The constituent filters consisted of a Butterworth filter applied to both the data, and time reversed data, thus forming a zero-phase filter. Zero-phase filters are intrinsically non-causal, which is problematic for real-time applications; attempts were made to replace these filters with causal filters, but the resulting phase shifts were extremely disruptive, rendering the filter useless. If the realtime removal of multipath is required, it may be possible (but beyond the scope of this paper) to use values of Θ from a previous sidereal day to remove it from the current data. It may also be possible (but, again, beyond the scope of this paper) to design causal transfer functions that work properly within the filter scheme.
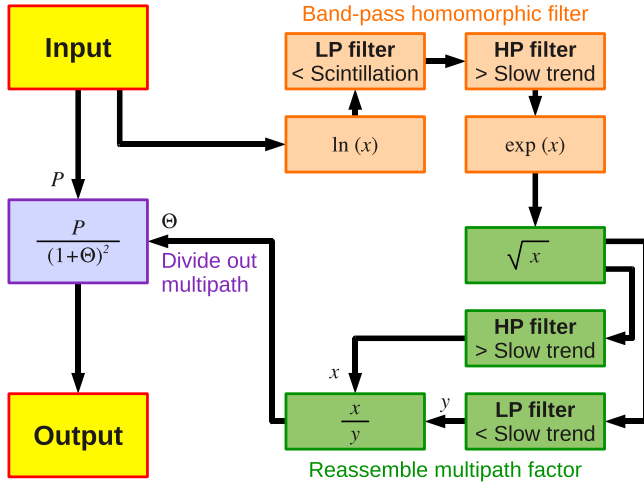
Figure 1. Filter scheme used to remove multipath induced power oscillation from GNSS data.

[25] When the algorithm was first implemented, it suffered from filter ringing, due to the mismatch between the non-zero edges of the data-set and the implicitly zero values outside of the data set. This problem was mitigated by using the reflection-padding technique, in which the edges of the data set were extended with a mirror image (in time) of the signal. This itself was imperfect, as the beginnings and the ends of data sets usually corresponded to a rising and a falling of the signal, and these were reversed by simple mirroring. Therefore, the mirrored signals were themselves turned upside-down in a logarithmic basis (and shifted upwards or downwards to form a continuous curve with the true signal) so that the rising and falling trends were maintained.

[26] The code was written using MatLab, with the Signal Processing Toolbox used to implement the filters.

3. Analysis of Multipath Environment

[27] The shape of the multipath induced power fringes contain information about the geometry of the sources of reflection. While this information is insufficient to completely reconstruct the receiver's surroundings, it can be used to constrain the likely positions of a reflector, even in the presence of other multipath sources. For example, if the multipath effect is believed to be from the ground, the technique can be used to verify that this is the case, as only a small fraction of possible multipath signal shapes are consistent with such a scenario.

[28] A variety of approaches have been applied to this problem. The most direct technique is to use a multiple antenna system, and to perform direction finding on the reflected signal [Axelrad et al., 1996; Comp and Axelrad, 1998; Santos and Farret, 2001; Farret and Santos, 2001]. This, however, requires specialist hardware, and can rarely be applied to third-party data. When using a single antenna, a simple technique (and one commonly built into GPS receiver software) is to record the satellite azimuth at the points of strong SNR oscillation, and then to assume that the reflector lies in the opposite direction [Hilla, 2004]. A more advanced method is to measure the multipath frequency by performing wavelet analysis on the SNR signal, and then to

match this frequency to that predicted from a model of planes tilted towards the receiver by an unknown angle [Bilich and Larson, 2007; Bilich et al., 2008]. Schemes based on carrier phase have also been used [Rost and Wanninger, 2009].

[29] In this section, a technique to constrain multipath reflectors based on the *shape* of the multipath signal (as isolated from other physical effects, using the filter in section 2) is described.

3.1. Multipath Geometry

[30] It is assumed that the surface of the object is locally planar, and that the reflection is specular. The reflection geometry can be represented using a vector $\vec{v}$ which points from the receiver to the tangential plane of the reflecting surface, such that $\vec{v}$ and the plane are perpendicular, as is shown in Figure 2. The direction of $\vec{v}$ doesn't necessarily point to the object itself. The law of specular reflection can be written as

$$\vec{\imath} - \vec{r} = 2(\vec{n} \cdot \vec{\imath})\vec{n} \tag{17}$$

where the unit vectors $\vec{\imath}$ and $\vec{r}$ give the directions of the incidence and reflected beams, and the unit vector $\vec{n}$ is perpendicular to the tangential plane. Using $\vec{r} = \vec{l_2}/|l_2|$ and $\vec{n} = -\vec{v}/|v|$ gives

$$\vec{\imath} - \frac{\vec{l_2}}{|l_2|} = \frac{2}{|v|^2}(\vec{v} \cdot \vec{\imath})\vec{v} \tag{18}$$

The observed interference pattern depends on the path difference

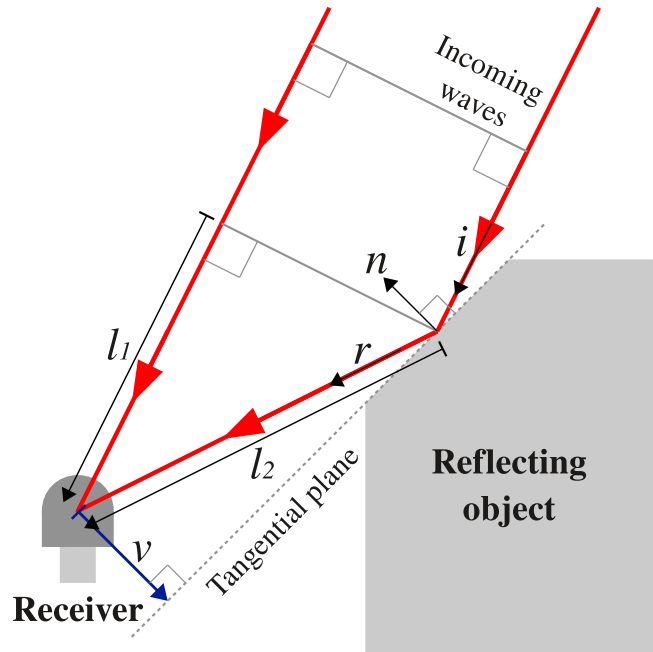$$d \equiv |l_2| - |l_1| \tag{19}$$

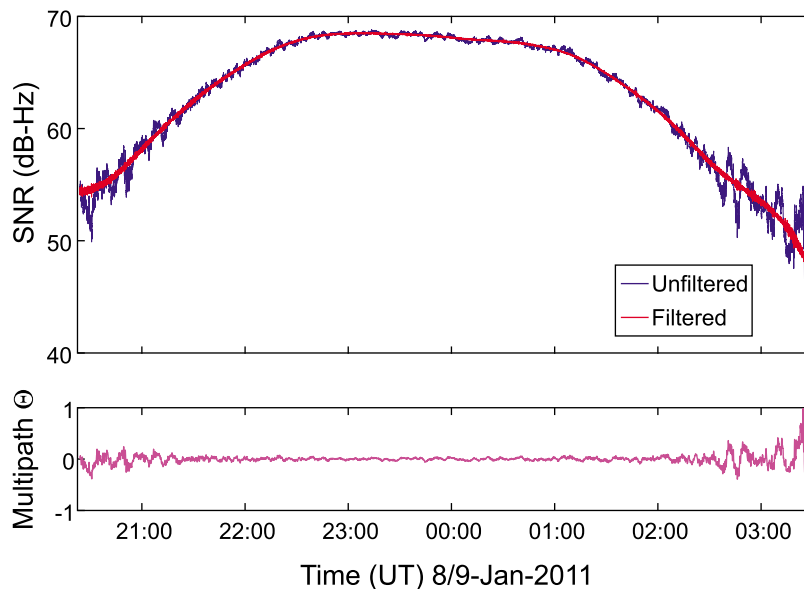**Figure 2.** Geometry of multipath, as parameterized with a perpendicular vector $\vec{v}$.

Figure 3. (top) Power data from GPS receiver, with and without multipath filter (PRN 27). (bottom) Multipath profile Θ extracted from data. The multipath filter isolates the band 0.00028 Hz to 0.067 Hz.

From the geometry in Figure 2, it can be seen that $|l_1| = \vec{\imath} \cdot \vec{l}_2$, and so

$$d = |l_2| - \vec{\imath} \cdot \vec{l}_2 \tag{20}$$

$$= -\vec{l}_2 \cdot \left(\vec{\imath} - \frac{\vec{l}_2}{|l_2|} \right) \tag{21}$$

Substituting equation (17) into equation (21) gives

$$d = -\frac{2}{|v|^2} \left(\vec{l}_2 \cdot \vec{v} \right) (\vec{\imath} \cdot \vec{v}) \tag{22}$$

From Figure 2, it can also be seen that $\vec{l}_2 \cdot \vec{v} = -|v|^2$. Substituting this in gives the relationship between path difference, satellite position and perpendicular vector as

$$d = 2\vec{v} \cdot \vec{\imath} \tag{23}$$

The rate of change of this path difference, in terms of wavelengths per unit time is given by

$$\nu = \frac{2}{\lambda} \vec{v} \cdot \frac{\mathrm{d}\vec{\imath}}{\mathrm{d}t} \tag{24}$$

A difference of one wavelength corresponds to a single cycle of power oscillation, and so ν is the frequency of the oscillation. The rate of change of direction is essentially an angular velocity, and can be split up as $\mathrm{d}\vec{\imath}/\mathrm{d}t = -\hat{w}\xi$, where ξ is the angular rate at which the satellite tracks across the sky, and $\hat{w}$ is a unit vector (perpendicular to $\hat{\imath}$) representing the apparent path at a given instant. This gives (on removing the physically irrelevant sign of the frequency)

$$\nu = \frac{2\xi}{\lambda} |\vec{v} \cdot \hat{w}| \tag{25}$$

which is the result discussed in section 2.1.

[31] The model assumes a single planar reflection, and so disregards the possibilities of multipath due to double reflections, multipath from curved surfaces and multipath due to diffraction. (If, however, the resulting multipath analysis reports the presence of a reflector which clearly doesn't exist, this provides some evidence that one of the above effects is present.)

[32] An additional problem is that trends in d differing uniformly by any integer multiple of the wavelength λ, will produce the same interference pattern. Therefore, only the change in distance Δd can be determined. The remaining d (mod λ) term *can* be extracted, but as d is usually much larger than λ, this quantity provides little useful information. This implies that reflectors with different geometries can produce similar interference patterns, and so from a given interference pattern, it is not possible to uniquely reconstruct the geometry.

3.2. Deriving Perpendicular Vectors With Spectral Analysis

[33] From equations (15) and (23), a set of ideal reflectors with perpendicular vectors $\vec{v}_n$, and reflectance coefficients ρ_n will have the form

$$\Theta_{\mathrm{model}}(\vec{v}_1, \vec{v}_2, \cdots, \vec{v}_N) = \sum_n \rho_n(t) \cos\left(\frac{4\pi}{\lambda} \vec{v}_n \cdot \vec{\imath}(t) \right) \tag{26}$$

In the simplified case of scalar v_n, and linear scalar $i(t)$, the reflector terms become sinusoids, and so can be resolved from a data set Θ by calculating the Fourier transform, and then determining v_n from the positions of the spectral peaks. In the proper case, a similar technique is possible, using a transform of the form

$$a(\vec{v}) = \int_{-\infty}^{\infty} \Theta(t) e^{j\left(\frac{4\pi}{\lambda} \vec{v} \cdot \vec{\imath}(t) \right)} \mathrm{d}t \tag{27}$$

where j is the unit imaginary. This is a generalization of the Fourier transform, and for the above simplified case, reduces
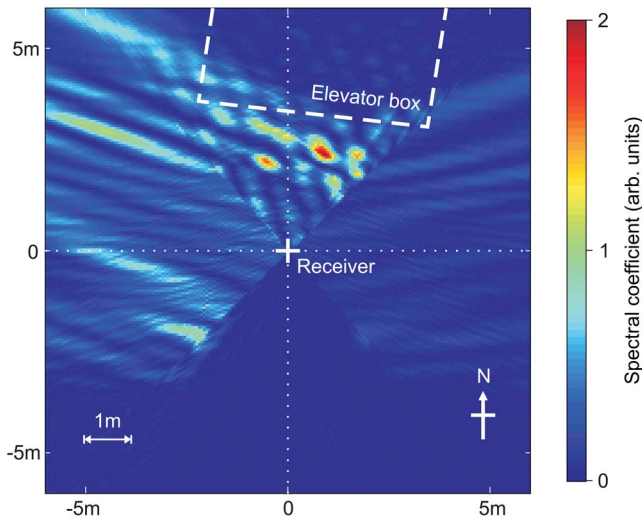
Figure 4. 2D spectral analysis of multipath (over horizontal plane), to locate reflectors in the signal shown in Figure 3.

to it. Like the Fourier transform, it is based on the principle that the product of two dissimilar waveforms will oscillate at a beat frequency, and so integrate to zero, whilst the product of two similar waveforms will retain a constant phase relationship, and so integrate to a nonzero value. This transform does not specifically extract the frequency, or any other readily definable characteristic of the signal. Instead, it is dependent on the signal's entire shape, and so makes use of all available information.

[34] Applying Euler's theorem to equation (27) gives

$$a(\vec{v}) = \int_{-\infty}^{\infty} \Theta(t) \cos\left(\frac{4\pi}{\lambda}\vec{v}\cdot\vec{\imath}(t)\right)\mathrm{d}t + j\int_{-\infty}^{\infty} \Theta(t) \sin\left(\frac{4\pi}{\lambda}\vec{v}\cdot\vec{\imath}(t)\right)\mathrm{d}t \tag{28}$$

In principle, only the real part is relevant, as the $\cos\left(4\pi\vec{v}\cdot\vec{\imath}/\lambda\right)$ kernel matches the functional form of the model, whilst the

imaginary part is a physically irrelevant quadrature term. In practice, however, the real part of the spectrum consists of wavelength-scale oscillations about each physical feature, due to the dependence of the interference pattern on relative phase. If a transform is calculated over a span of meters or tens of meters, this ultra-fine detail is a nuisance, as to avoid aliasing, the transform resolution is kept impractically high. A better option is to consider the absolute value of the transform, and thus remove these phase oscillations.

[35] Another practical issue is that any real measurement will have a finite time span (instead of the infinite range specified in equation (27)). This was dealt with by assuming all values outside of the recorded range to be zero.

[36] The ρ_n coefficients are themselves time varying, and so will influence the spectrum. However, the functional form is likely be a temporally broad hump, and so the spectrum is likely to be a spectrally narrow hump centered about the origin. (For example the Fourier transform of a wide Gaussian function is a narrow Gaussian function.) In the spectral domain, the multiplication by ρ_n becomes a convolution by its spectrum. Therefore, the only outcome is a small spectral broadening of the features corresponding to reflectors. The coefficients are also dependent on the antenna gain pattern, but again, due to the slowly varying nature, this will have little effect on the spectral analysis. It is only if the reflection coefficients are to be themselves measured (which is beyond the scope of this paper) that the gain pattern must be analyzed.

[37] The most important problem is that previously mentioned, of trends in d differing uniformly by any integer multiple of the wavelength λ producing the same interference pattern. It is pointless to perform a 3D transform, as a single reflector will appear to be located over a range of positions. As is explained in Appendix B, a 2D transform is possible (for example by assuming the perpendicular vector to be horizontal). Each point derived from the transform $\vec{v}_n$ can then be (approximately) extended to a 1D set of points as

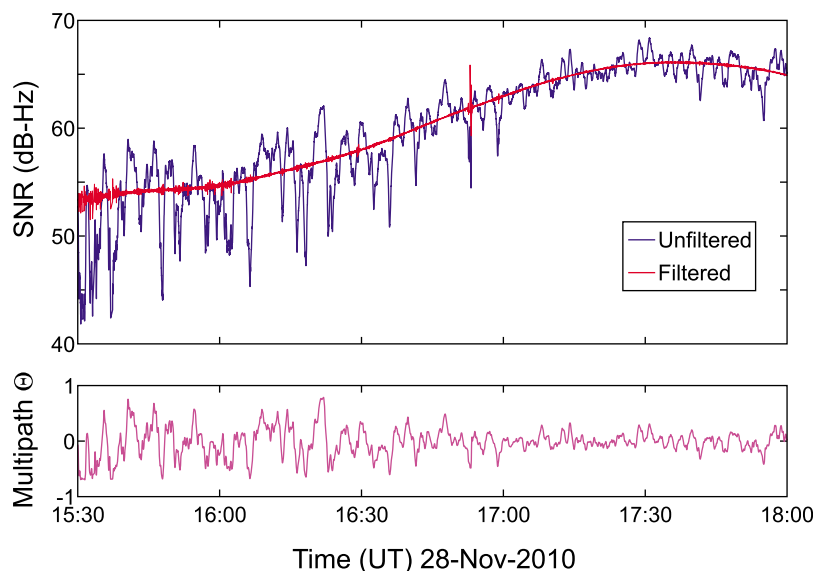$$\vec{v}_n' = \vec{v}_n + \gamma_n \vec{g} \tag{29}$$

Figure 5. (top) Power data from GPS receiver, with and without multipath filter (PRN 32). (bottom) Multipath profile Θ extracted from data. The multipath filter isolates the band 0.00028 Hz to 0.067 Hz.
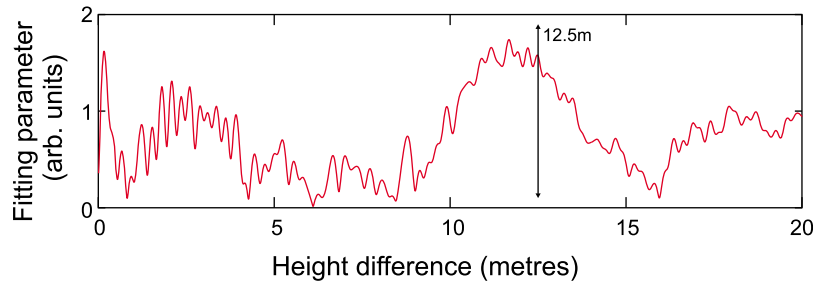
Figure 6. 1D spectral analysis of multipath (over vertical line) to locate reflectors in the signal shown in Figure 5. A spectral peak is visible in close proximity to the 12.5 m depth of a ledge.

where is γ_n is a free coefficient for each reflector, and $\vec{g}$ is a common vector, which is derived from the satellite track across the sky. In general $\vec{g}$ will point in a direction which is neither horizontal nor vertical, and so if a reflector is thought to be at a particular position, it is improbable (at least in most environments) that another realistic reflector will lie at any other point along $\vec{v}_n$. (In the case studies described below, no such alternative reflectors were seen.)

4. Results

[38] Three case studies, all using GPS, were investigated. In each case, a NovAtel GPStation 2, sampling at 50 Hz was used. The raw data were filtered (to remove occasional instances of unphysically large or identically zero values) and then down-sampled to 1 Hz by calculating the mean (of linearly scaled data) over 50 sample bins. The filter frequencies (shown in the relevant figure captions) were chosen by visual inspection of graphs of the input and filtered data. The upper bound to the multipath frequency window was steadily increased until either no trace of the multipath oscillations remained, or further increase gave no improvement. The lower frequency was steadily decreased,

until the filtered curve passed neatly through the inflection points of the oscillations in the unfiltered curve.

4.1. Simple Multipath Environment

[39] An antenna was placed on a roof, several meters away from a machinery box capping an elevator shaft. Strong multipath peaks were recorded, as is shown in Figure 3. A 2D spectral analysis was performed on the Θ parameter extracted from the data (over its entire time range), as shown in Figure 4. This clearly shows a strong spectral peak, corresponding to a vector perpendicular to the elevator box wall. There are also some weaker peaks in the same direction, the origin of which are not known. It is possible that some double reflections are present. It is also possible that some spurious frequencies have entered the signal; these may be due to nonlinearity in the receiver causing frequency mixing, or deviations from the assumptions made by the filter scheme having a non-trivial effect.

4.2. Complex and Noisy Multipath Environment

[40] An antenna was placed in a courtyard, in a metal framed building, with metalized glass windows, providing a complex multipath environment. Many satellites were visible
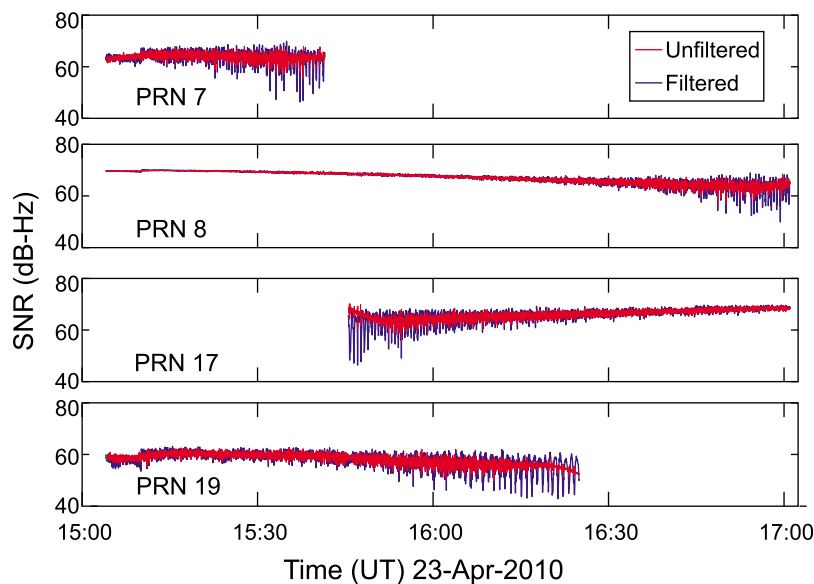

Figure 7. Signals taken from Flamborough Head. The multipath filter isolates the band 0.0011 Hz to 0.1 Hz.
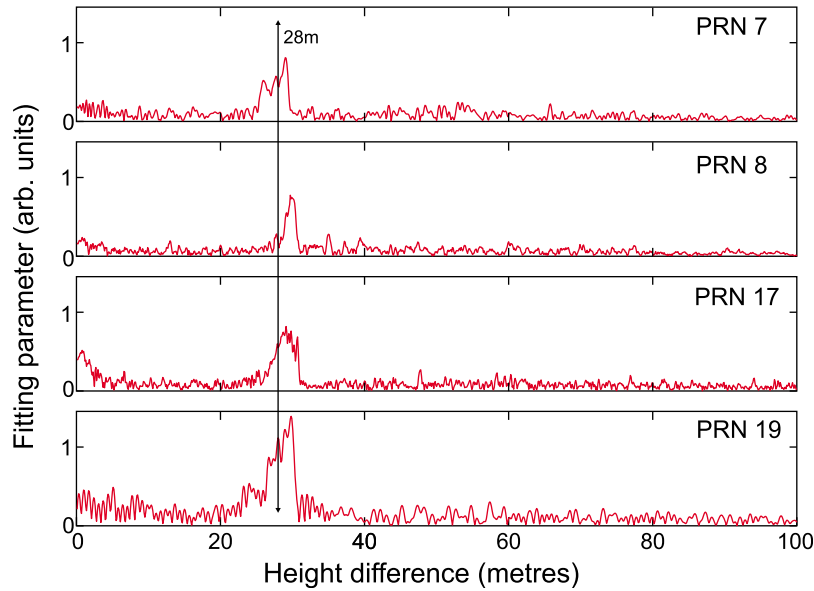
Figure 8. Estimate of height difference between receiver and sea level at Flamborough Head. Spectral peaks are visible in close proximity to the 28 m measured height.

despite being occluded by buildings for their entire pass. The result (as shown for satellite PRN 32 in Figure 5) was a very complex signal lacking any obvious periodicity. Despite this complexity, reflection from a flat ledge (measured to be 12.5 m below the receiver) could be detected in a spectral plot of vertical $\vec{v}$ vectors (calculated over the entire time interval), as is shown in Figure 6.

4.3. Satellites Rising and Setting Over Sea

[41] An antenna was placed on a coastal cliff top at Flamborough Head (54° 06′ 59″ N; 0° 04′ 58″ W), over-looking the North Sea, with a northerly to easterly view. Three GPS satellites (PRNs 7, 8, and 19) were observed setting over the sea, and a fourth (PRN 17) was observed

rising. For all four satellites, pronounced interference fringes were seen (as is shown in Figure 7). Spectral analysis was performed over the entire available time intervals, for vertical vectors with lengths ranging from 0 to 100 meters, as is shown in Figure 8). The variation in the available time intervals have a moderate effect on the width of the spectral peaks. The plot corresponding to the longest time interval (for PRN 8) has the narrowest spectral peak width, an effect which is analogous to the Fourier scaling theorem. The antenna was measured (using a laser range-finder) to be 28 m above sea level. This height matches the peaks to within 2m in all four plots.

[42] An antenna was placed in Boulby (54° 33′ 58″ N; 0° 50′ 27″ W), also on cliffs overlooking the North Sea, with a northerly to easterly view. Very rapid multipath fringes
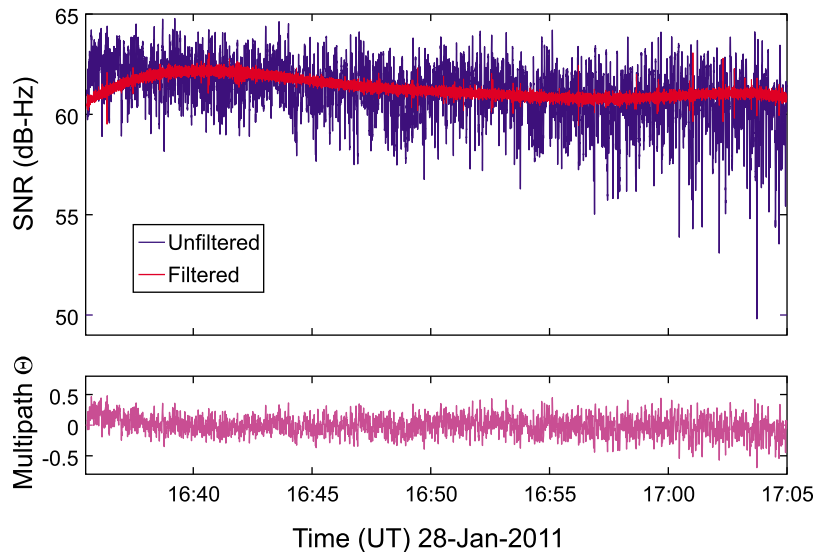

Figure 9. Signal taken from Boulby, for PRN 30. The multipath filter isolates the band 0.0011 Hz to 1 Hz.
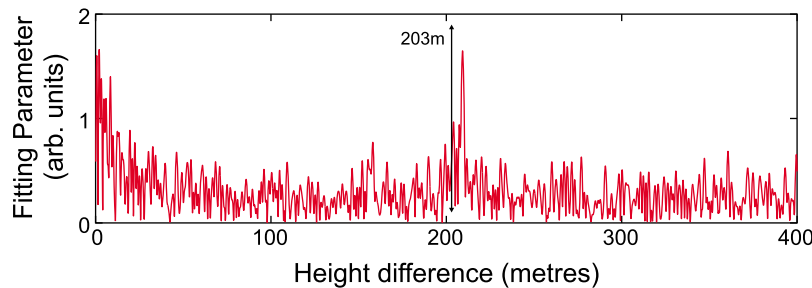
Figure 10. Estimate of height difference between receiver and sea level at Boulby. A spectral peak is visible in close proximity to the 203 m map height.

were seen, as is shown in Figure 9. (In this case, it was necessary to reduce the sample binning to 5 samples per bin, thus providing a 10Hz data rate.) By performing spectral analysis (over the entire time interval) for PRN 30, a reflection peak at 209 m was seen (as is shown in Figure 10) which is within 3% of the 203 m height given by the Ordnance Survey.

5. Conclusions

[43] A filter to separate the effect of multipath from GNSS signal-to-noise ratio data was developed and applied to a variety of cases. In all cases, the filtered data was shown to preserve slowly varying trends, resulting from effects such as tropospheric absorption, antenna anisotropy and variations in satellite range.

[44] The filtered data also retained high frequency components, leaving it suitable for geophysical work such as detecting ionospheric amplitude scintillation. A potential application is in "detrending" the data used to calculate amplitude scintillation metrics, such as the S4 index. This is normally done by dividing the signal by the output of a linear low-pass filter [*Van Dierendonck et al.*, 1993], to remove multipath along with the above slowly varying effects. A more physically realistic approach would be to remove the multipath first, using the described filter. A detailed study on this will be the focus of a future paper.

[45] Similarly, the multipath data extracted from the input data is minimally distorted, and so contains information describing the multipath geometry. Unlike other multipath analysis schemes, it has been cleanly separated from other effects, using a method which fully accounts for the physical nature of the phenomenon. The cleanness of the data allows it to be analyzed to constrain the source of the multipath reflector, and a scheme to perform this analysis has been presented. The scheme has been shown to successfully reconstruct the height of coastal cliffs, the depth of a courtyard, and the orientation of a rooftop reflector.

Appendix A: Zero Frequency Component of $f = \ln(1 + \sum_n \alpha_n \cos\theta_n)$

[46] In Appendix A, the zero-frequency (DC) component of the function $f = \ln(1 + \sum_n \alpha_n \cos\theta_n)$ is derived. Taylor expanding the log function about unity gives

$$\ln\left(1 + \sum_n \alpha_n \cos\theta_n\right) = \sum_{l=1}^{\infty} \frac{(-1)^{l+1}}{l} \sum_n \alpha^l \cos^l(\theta_n) \quad (A1)$$

This is the sum of sinusoidal terms and constant terms (which result from the expansion of even powers of the cosine function). The zero frequency component of f is the sum of these constant terms, which (for even l) are given by

$$\left[\cos^l(\theta)\right]_{\text{DC}} = \frac{l!}{2^l \left(\frac{1}{2}l\right)!^2} \quad (A2)$$

Making the change of variable $l = 2m$ gives

$$\left[\cos^m(\theta)\right]_{\text{DC}} = \frac{(2m)!}{2^{2m} m!^2} \quad (A3)$$

Thus giving a sum of the form

$$\left[\ln\left(1 + \sum_n \alpha_n \cos\theta_n\right)\right]_{\text{DC}} = \sum_n \sum_{m=1}^{\infty} \frac{-(2m)!}{2m2^{2m}m!^2} \alpha_n^{2m} \quad (A4)$$

Using the summing formula

$$\sum_{m=1}^{\infty} \frac{(2m)!}{2m2^{2m}m!^2} \alpha^{2m} = -\ln\left(\frac{1 + \sqrt{1 - \alpha^2}}{2}\right) \quad (A5)$$

(which can be derived by noting that the left-hand-side is the Taylor series about $\alpha = 0$ of the right-hand-side) gives the final result as

$$\left[\ln\left(1 + \sum_n \alpha_n \cos\theta_n\right)\right]_{\text{DC}} = \sum_n \ln\left(\frac{1 + \sqrt{1 - \alpha_n^2}}{2}\right) \quad (A6)$$

Appendix B: Relationship Between Perpendicular Vectors Corresponding to Same Interference Pattern

[47] In Appendix B, an approximate formula relating the different perpendicular vectors giving rise to the same interference pattern is derived. In matrix notation, using Cartesian coordinates, equation (23) becomes

$$d = 2\begin{bmatrix} v_x & v_y & v_z \end{bmatrix} \begin{bmatrix} i_x \\ i_y \\ i_z \end{bmatrix} \quad (B1)$$

The direction of the incoming satellite signal at a time t was parameterized by applying an Affine transformation (defined

with matrix $\hat{A}$ and column vector $\vec{b}$) to a vector function of time $\vec{x}(t)$ representing a simple basis rotation, such that

$$\begin{bmatrix} i_x \\ i_y \\ i_z \end{bmatrix} = \hat{A}\vec{x}(t) + \vec{b} \qquad (B2)$$

A basis of the form

$$\vec{x}(t) = \frac{1}{\sqrt{2}}[\cos(\Omega t) \sin(\Omega t) \, 1]^{\mathrm{T}} \qquad (B3)$$

was chosen, with Ω being used as additional fitting parameter. The least-squares best-fit values of $\hat{A}$ and $\vec{b}$ were derived at given values of Ω using the method described by *Spath* [2004]. (In practice, the transformation will be similar to an orthogonal transformation, due to the requirement that the fitted values of $\vec{\imath}$ approximate unit vectors.) The fitting coefficient was then minimized in Ω (using a golden-section method) to find the overall least-squares best-fit. Typically, when fitting an entire satellite pass with data at one minute intervals, the real and fitted coordinates matched to within less than a degree. Combining equations (B1)–(B3) (and taking the transpose) gives

$$d = \sqrt{2}\,[\cos(\Omega t) \sin(\Omega t) \, 1]\hat{A}^{\mathrm{T}}\begin{bmatrix} v_x \\ v_y \\ v_z \end{bmatrix} + 2\vec{b}^{\mathrm{T}}\begin{bmatrix} v_x \\ v_y \\ v_z \end{bmatrix} \qquad (B4)$$

Then, by defining

$$\begin{bmatrix} \alpha \\ \beta \\ \gamma \end{bmatrix} = \hat{A}^{\mathrm{T}}\begin{bmatrix} v_x \\ v_y \\ v_z \end{bmatrix} \qquad (B5)$$

the path length is given by

$$d = \sqrt{2}(\alpha\cos(\Omega t) + \beta\sin(\Omega t) + \gamma) + 2\vec{b}^{\mathrm{T}}(\hat{A}^{\mathrm{T}})^{-1}[\alpha \, \beta \, \gamma]^{\mathrm{T}} \quad (B6)$$

It is at this point that the interference problem becomes relevant. Any constant term is practically unmeasurable (due to an integer wavelength offset having no effect on the interference pattern), and so it is removed to give

$$\Delta d = \sqrt{2}(\alpha\cos(\Omega t) + \beta\sin(\Omega t)) \qquad (B7)$$

This formulation makes the resulting ambiguity explicit, as the coefficient γ is now missing (and so immeasurable), whilst the other two coefficients α and β still remain. The fact that one degree of freedom has been lost means that it is only meaningful to do spectral analysis of the multipath signal in one or two dimensions. Inverting equation (B5), and decomposing the vector into known and unknown components gives

$$\begin{bmatrix} v_x \\ v_y \\ v_z \end{bmatrix} = (\hat{A}^{\mathrm{T}})^{-1}\begin{bmatrix} \alpha \\ \beta \\ 0 \end{bmatrix} + \gamma(\hat{A}^{\mathrm{T}})^{-1}\begin{bmatrix} 0 \\ 0 \\ 1 \end{bmatrix} \qquad (B8)$$

The first term on the right-hand-side is known, whilst the second term corresponds to a vector with known direction,

but unknown scale γ. It therefore follows that a spectral analysis reporting a reflector with perpendicular vector $\vec{v}$ is in fact consistent with a set of vectors given by

$$\vec{v}' = \vec{v} + \gamma\vec{g} \qquad (B9)$$

where the direction of the path along which the perpendicular vector may lie is (subject to the approximations made in fitting the satellite data) given by

$$\vec{g} = (\hat{A}^{\mathrm{T}})^{-1}\begin{bmatrix} 0 \\ 0 \\ 1 \end{bmatrix} \qquad (B10)$$

References

Axelrad, P., C. Comp, and P. MacDoran (1994), Use of signal-to-noise ratio for multipath error correction in GPS differential phase measurements: Methodology and experimental results, paper presented at the 7th International Technical Meeting of the Satellite Division of the Institute of Navigation, Salt Lake City, Utah.

Axelrad, P., C. J. Comp, and P. F. Macdoran (1996), SNR-based multipath error correction for GPS differential phase, *IEEE Trans. Aerosp. Electron. Syst.*, *32*, 650–660.

Beach, T. L., and P. M. Kintner (1999), Simultaneous global positioning system observations of equatorial scintillations and total electron content fluctuations, *J. Geophys. Res.*, *104*, 22,553–22,565.

Bilich, A., and K. M. Larson (2007), Mapping the GPS multipath environment using the signal-to-noise ratio (SNR), *Radio Sci.*, *42*, RS6003, doi:10.1029/2007RS003652.

Bilich, A., P. Axelrad, and K. M. Larson (2007), Scientific utility of the signal-to-noise ratio (SNR) reported by geodetic GPS receivers, paper presented at ION GNSS, Fort Worth, Tex., 26–28 Sept.

Bilich, A., K. M. Larson, and P. Axelrad (2008), Modeling GPS phase multipath with SNR: Case study from the Salar de Uyuni, Boliva, *J. Geophys. Res.*, *113*, B04401, doi:10.1029/2007JB005194.

Comp, C. J., and P. Axelrad (1998), Adaptive SNR-based carrier phase multipath mitigation technique, *IEEE Trans. Aerosp. Electron. Syst.*, *34*, 264–276.

Dai, D., T. Walter, C. J. Comp, Y. J. Tsai, P. Y. Ko, P. K. Enge, and J. D. Powell (1997), High integrity multipath mitigation techniques for ground reference stations, paper presented at 10th International Technical Meeting, Satell. Div., Inst. of Navig., Kansas City, Mo.

Farret, J. C., and M. C. Santos (2001), An alternative method for detection and mitigation of static multipath in L1 carrier phase measurements, paper presented at ION National Technical Meeting, Inst. of Navig., Long Beach, Calif., 22–24 Jan.

Forte, B. (2005), Optimum detrending of raw GPS data for scintillation measurements at auroral latitudes, *J. Atmos. Sol. Terr. Phys.*, *67*, 1100–1109.

Hilla, S. (2004), Plotting pseudorange multipath with respect to satellite azimuth and elevation, *GPS Solut.*, *8*, 44–48.

Kaplan, E. D., and C. J. Hegarty (2006), *GPS Principles and Applications*, Artech House, Boston, Mass.

Larson, K. M., E. E. Small, E. D. Gutmann, A. L. Bilich, J. J. Braun, and V. U. Zavorotny (2008a), Use of GPS receivers as a soil moisture network for water cycle studies, *Geophys. Res. Lett.*, *35*, L24405, doi:10.1029/2008GL036013.

Larson, K. M., E. E. Small, E. Gutmann, A. Bilich, P. Axelrad, and J. Braun (2008b), Using GPS multipath to measure soil moisture fluctuations: Initial results, *GPS Solut.*, *12*, 173–177.

Larson, K. M., J. J. Braun, E. E. Small, V. U. Zavorotny, E. D. Gutmann, and A. L. Bilich (2010), GPS multipath and its relation to near-surface soil moisture content, *IEEE J. Sel. Top. Appl. Earth Obs. Remote Sens.*, *3*, 91–99.

Rost, C., and L. Wanninger (2009), Carrier phase multipath mitigation based on GNSS signal quality measurements, *J. Appl. Geod.*, *3*, 1–8.

Santos, M. C., and J. C. F. Farret (2001), Detection and mitigation of static multipath in L1 carrier phase measurements using a dual-antenna approach, paper presented at IAG Scientific Assembly, Int. Assoc. of Geod., Budapest, 2–7 Sept.

Spath, H. (2004), Fitting affine and orthogonal transformations between two sets of points, *Math. Commun.*, *9*, 27–34.

Van Dierendonck, A. J., J. Klobuchar, and Q. Hua (1993), Ionospheric scintillation monitoring using commercial single frequency C/A code receivers, paper presented at the 6th International Technical Meeting of the Satellite Division of the Institute of Navigation, Salt Lake City, Utah.

Wang, W., J. Cai, D. Zeng, and X. Dong (2008), Generalized cepstrum correlation function analysis method on multipath signals of GPS, *J. Acad. Equip. Command Technol.*, *19*, 71–75.

Ying, Z., Y. Xiaofan, T. Bin, and Y. Kechu (2003), An anti-multipath-fading algorithm based on cepstrum analysis, *Signal Process.*, *19*, 55–58.

C. J. Benton and C. N. Mitchell, Department of Electronic and Electrical Engineering, University of Bath, Claverton Down, Bath BA2 7AY, UK. (c.j.benton@bath.ac.uk; c.n.mitchell@bath.ac.uk)